The phosphorylated redox proteome of *Chlamydomonas reinhardtii*: Revealing novel means for regulation of protein structure and function

Evan W. McConnell, Emily G. Werth, Leslie M. Hicks*

Department of Chemistry, University of North Carolina at Chapel Hill, Chapel Hill, NC, United States

ABSTRACT

Post-translational modifications (PTMs) are covalent modifications to protein residues which may alter both conformation and activity, thereby modulating signaling and metabolic processes. While PTMs have been largely investigated independently, examination into how different modification interact, or crosstalk, will reveal a more complete understanding of the reciprocity of signaling cascades across numerous pathways. Combinatorial reversible thiol oxidation and phosphorylation in eukaryotes is largely recognized, but rigorous approaches for experimental discovery are underdeveloped. To begin meaningful interrogation of PTM crosstalk in systems biology research, knowledge of targeted proteins must be advanced. Herein, we demonstrate protein-level enrichment of reversibly oxidized proteoforms in *Chlamydomonas reinhardtii* with subsequent phosphopeptide analysis to determine the extent of phosphorylation in the redox thiol proteome. Label-free quantification was used to quantify 3353 oxidized Cys-sites on 1457 enriched proteins, where sequential phosphopeptide enrichment measured 1094 sites of phosphorylation on 720 proteins with 23% (172 proteins) also identified as reversibly oxidized. Proteins identified with both reversible oxidation and phosphorylation were involved in signaling transduction, ribosome and translation-related machinery, and metabolic pathways. Several redox-modified Calvin-Benson cycle proteins were found phosphorylated and many kinases/phosphatases involved in phosphorylation-dependent photosynthetic state transition and stress-response pathways had sites of reversible oxidation. Identification of redox proteins serves as a crucial element in understanding stress response in photosynthetic organisms and beyond, whereby knowing the ensemble of modifications co-occurring with oxidation highlights novel mechanisms for cellular control.

1. Introduction

PTMs are covalent modifications to the primary structure of proteins and are necessary for the regulation of critical processes including metabolism, signaling, and overall homeostasis [1,2]. Phosphorylation is a reversible modification to amino acid residues (primarily Ser, Thr, and Tyr) catalyzed by protein kinases and removed by phosphatases, which can trigger structural changes of proteins to alter diverse biological properties [3]. Likewise, the reversible oxidation of protein cysteine thiols (-SH) has emerged as a principal regulatory mediator akin to phosphorylation by forming highly distinct redox switches including disulfide bridges (-SSR) [4], *S*-glutathionylation (-SSG) [5], S-nitrosylation (-SNO) [6], and *S*-sulfenylation (-SOH) [7]. Under conditions of adverse oxidative stress, irreversible sulfinic (-SO$_2$H) and

sulfonic (-SO$_3$H) acids may develop *via* sequential oxidation of sulfenylated thiols [8]. Collectively, both phosphorylation and reversible thiol oxidation represent molecular switches that may fine-tune the functional response of proteins involved in many crucial processes [9].

While both modifications have been largely investigated independently, examination into how they interact, or crosstalk, will reveal a more complete understanding of the reciprocity of signaling cascades across numerous pathways [10]. Recent advances in proteome-wide studies of methionine oxidation in *Arabidopsis thaliana* have shown that it may serve as a rheostat to control the phosphorylation of proximal residues, further revealing the widespread consequences of redox signaling [11,12]. Similarly, proteins with both reversible cysteine oxidation and phosphorylation sites are largely recognized [13,14], yet studies identifying proteoforms simultaneously affected by

these modifications are sparse [15,16]. Discovery and targeted validation of these PTMs and the effect on protein structure and function are particularly lacking for photosynthetic organisms and must be advanced to begin meaningful definition of signaling pathways [17].

Chlamydomonas reinhardtii (hereafter, Chlamydomonas) is an extensively studied microalgae and serves as a model for fundamental biological processes, including photosynthesis, flagellar development, and triacylglycerol accumulation [18]. Several large-scale proteomic studies have mapped the extent of reversibly oxidized Cys in the Chlamydomonas proteome. Zaffagnini et al. [19] identified 225 glutathionylated proteins using biotinylated glutathione and streptavidin affinity chromatography, additionally mapping 56 glutathionylated Cys-sites using peptide affinity purification and tandem mass spectrometry. Morisse et al. [20] used complementary enrichment methods to identify 492 proteins with potential sites of S-nitrosylation. Recently, Pérez-Pérez et al. [21] determined TRX targets in Chlamydomonas to show 1188 proteins actively modulated by TRX-dependent reduction of disulfide bonds. Our research group has benchmarked the use of thiol-affinity resin to enrich peptides from reversibly oxidized proteins in photosynthetic organisms, notably using label-free quantification to measure the abundance of 3662 redox Cys-containing peptides from 1924 proteins in Chlamydomonas [22].

There has also been considerable interest in studying the extent of phosphorylation in the Chlamydomonas proteome. Wagner et al. [23] identified 360 phosphopeptides from 328 different proteins in Chlamydomonas treated with Ser/Thr phosphatase inhibitors, while Pan et al. [24] isolated flagella to determine phosphorylation events on 224 proteins involved with motility and assembly. We comprehensively analyzed the global Chlamydomonas phosphoproteome by localizing 15,862 phosphosites on 4588 proteins and enhanced the understanding of a range of regulatory mechanisms controlling photosynthesis, carbon assimilation, glycolysis, and other distinct cellular processes [25]. Our efforts to quantify the phosphoproteome used a dual enrichment strategy that targeted intact protein kinases by capture on immobilized multiplexed kinase inhibitor beads with subsequent proteolytic digestion of unbound proteins and peptide-based phosphorylation enrichment [26], thereby measuring the abundance of 2250 phosphosites across 1055 proteins.

Reversible oxidation and phosphorylation alone are key regulators in Chlamydomonas metabolic and signaling pathways, but it is not well-known the extent of proteins co-occupied by both modifications. Prior studies to broadly identify proteins with both Cys and phosphorylated residues have relied on performing some variation of phosphorylation enrichment on Cys-containing peptides enriched with thiol-affinity resin [27,28]. As a result of a peptide-based enrichment, these approaches were limited to identifying dually-modified proteins only if tryptic peptides contained both PTMs without a cleavage site between the affected residues. An alternative method used cysteine-specific phosphonate adaptable tags to simultaneously enrich peptides with either tagged Cys residues, phosphorylation, or combinations thereof [29], noting from the low frequency of doubly-modified peptides that these PTMs must generally coexist on distant residues in the protein sequence, implying an approach targeting intact proteins would be better-suited. We previously developed a two-dimensional electrophoresis strategy for parallel analysis of changes to the redox, phosphorylated, and total proteome using spectrally distinct fluorophores, which was used to study the chemical inhibition of the target of rapamycin (TOR) signaling pathway in Chlamydomonas [30].

Herein, we present a method for protein enrichment of reversibly oxidized proteoforms with subsequent phosphopeptide analysis to determine the extent of phosphorylation in the redox thiol proteome. Thiol-affinity resin was used to enrich intact proteins with reversible oxidation prior to enzymatic digestion. Following on-resin digestion and stoichiometric recombination of eluate and flow-through, phosphopeptide enrichment was performed to identify phosphosites on reversibly oxidized proteoforms. This approach allowed detection of reversibly oxidized proteins and the ensemble of additional phosphorylation on the redox proteome. We demonstrated biological significance of this approach in a model photosynthetic organism, *Chlamydomonas reinhardtii*, and quantified 3353 reversibly oxidized Cys on 1457 proteins and 1094 phosphorylation sites on 720 proteins, thereby providing broad, site-specific coverage of the proteome affected by both reversible oxidation and concurrent phosphorylation.

2. Materials and methods

2.1. Preparation of biological material

Wild-type *Chlamydomonas reinhardtii* strain CC-2895 6145c mt- was purchased from the Chlamydomonas Resource Center (www.chlamycollection.org). Cells were cultivated photoheterotrophically in 250 mL flasks holding 100 mL of Tris-acetate-phosphate medium [31]. Cultures were maintained at 22 °C on an Innova 2000 platform shaker (New Brunswick Scientific, Enfield, CT, USA) at 120 rpm under $100 \,\mu mol \,m^{-2} \,s^{-1}$ illumination with a 12 h photoperiod. For all experiments, biological replicates were simultaneously grown to mid-log phase (OD_{750} 0.4–0.5) and harvested 2 h after the dark-light transition. Cells were harvested by centrifuging for 5 min at $2000 \times g$ and discarding the supernatant. Cell pellets were flash-frozen using liquid nitrogen and stored at − 80 °C until use.

2.2. Protein extraction

Unless noted, all steps were performed on ice under low light conditions. Cell pellets (0.3 g) were resuspended in 3 mL of lysis buffer containing 50 mM Tris, pH 8.0 with 1 mM diethylenetriaminepentaacetic acid (DTPA), 0.1 mM neocuproine, 100 mM iodoacetamide (IAM), and 1 × concentrations of cOmplete protease inhibitor and phosSTOP phosphatase inhibitor cocktails (Roche, Indianapolis, IN, USA). To avoid bubbling, 0.5% Triton X-100 was added immediately following pellet resuspension. Cells were lysed *via* sonication using an E220 focused-ultrasonicator (Covaris, Woburn, MA, USA) for 2 cycles of 30 s at 200 cycles/burst, 100 W power, and 13% duty cycle. Following sonication, 2% SDS was added to the homogenate and alkylation was continued in a Thermomixer (Thermo Fisher Scientific, Rockford, IL, USA) for 2 h protected from light at 50 °C and 850 rpm. Cellular debris was cleared by centrifugation for 5 min at $20,000 \times g$ and proteins were precipitated from the supernatant using 5 volumes of cold 100 mM ammonium acetate in methanol. Following incubation for 30 min at − 80 °C, proteins were pelleted by centrifugation for 5 min at $2000 \times g$. To remove excess reagents, the pellet was washed with 100 mM ammonium acetate in methanol and once with 70% ethanol. Precipitate was resuspended in 1 mL of 50 mM Tris-HCl, pH 8.0 with 0.5% SDS, and 8 M urea and remaining cellular debris was removed by centrifugation. Protein concentrations were determined using the CB-X assay (G-Biosciences, St. Louis, MO, USA) against BSA standard. Reversibly oxidized thiols were reduced using 10 mM dithiothreitol (DTT) and incubated in a Thermomixer for 1 h at 30 °C and 850 rpm. Excess DTT was removed by loading protein sample to an Amicon Ultra-2 centrifugal filter (EMD Millipore, Billerica, MA, USA) with 10 kDa MWCO and centrifuging for 10 min at 4 °C and $10,000 \times g$. Buffer exchange proceeded by adding 1 mL of 50 mM Tris, pH 8.0 with 1 mM DTPA and 0.5% SDS in two passes. Protein was recovered from the filter using an equal volume of washing buffer and estimated for concentration. A negative control for reversible oxidation samples was prepared by combining an aliquot from each replicate and processing identically as above without the addition of DTT reductant. Subsequent enrichment of nascent thiols was performed using 1 mg of protein lysate at 2 mg/mL concentration.

2.3. Protein-level cysteine enrichment

Thiopropyl Sepharose 6B resin (GE Healthcare Bio-Sciences, Pittsburgh, PA, USA) was rehydrated in water and washed twice in batch mode using washing buffer containing 50 mM Tris, pH 8 with 1 mM DTPA. Per replicate, 1 mg of protein sample (*i.e.*, 500 µL of a 2 mg/mL lysate) was loaded to 50 mg of resin (*i.e.*, 500 µL of a 100 mg/mL slurry) in a MobiSpin column (MoBiTec GmbH, Göettingen, Germany) and incubated in a Thermomixer for 2 h at 30 °C and 850 rpm to enrich proteins with reduced cysteine thiols. Nonspecifically bound proteins were removed by washing the resin twice with ten bed volumes each of washing buffer with 0.5% SDS, washing buffer with 2 M NaCl, 70% acetonitrile with 0.1% trifluoroacetic acid (TFA), and finally 50 mM Tris-HCl, pH 8. On-resin digestion of Cys-bound proteins was performed by resuspending protein-resin slurry in 500 µL of 50 mM Tris, pH 8 before adding 10 µg of Trypsin Gold (Promega, Madison, WI, USA). The mixture was incubated in a Thermomixer for 3 h at 37 °C and 850 rpm before collecting peptide flow-through from bound Cys-proteins *via* brief centrifugation. Samples were then washed with ten bed volumes each of washing buffer with 2 M NaCl, 70% acetonitrile with 0.1% TFA, and 50 mM Tris-HCl, pH 8. Bound Cys-containing peptides were eluted from the resin twice using 250 µL of 10 mM Tris, pH 8.0 with 50 mM DTT for 15 min. Samples for sequential enrichment of phosphopeptides were prepared by dividing both the eluate and flow-through in half. One portion of eluate was directly processed for redox Cys profiling, while the other was combined with one portion of flow-through to represent an equal stoichiometry of an intact digest of Cys-bound proteins.

2.4. Solid-phase extraction (SPE) desalting

Desalting of samples was performed using 50 mg/1.0 mL Sep-Pak C18 cartridges (Waters) held in a SPE 24-position vacuum manifold (Phenomenex, Torrance, CA, USA) at a flow rate of 1 drop/s. Resin was first pre-eluted using 1 mL of 80% acetonitrile with 0.1% TFA before equilibration with 1 mL of water with 0.1% TFA. Samples were acidified to pH 3 using 5% TFA and loaded onto the cartridges in three passes and then washed using 1 mL of water with 0.1% TFA. Peptides were eluted using 1 mL of 80% acetonitrile with 0.1% TFA and concentrated by vacuum centrifugation.

2.5. Phosphopeptide enrichment

Following solid-phase extraction and vacuum centrifugation, samples were resuspended in 200 µL of 80% acetonitrile with 1% TFA and 25 mg/mL phthalic acid. Phosphopeptide enrichment was performed using 1 mg/10 µL Titansphere Phos-TiO tips (GL Sciences, Torrance, CA, USA). The resin was pre-eluted using 20% acetonitrile with 5% ammonium hydroxide and centrifuged for 2 min at 1000 × g before conditioning in 80% acetonitrile with 1% TFA. Samples were loaded to the tips in three passes and then washed in four passes using 80% acetonitrile with 1% TFA to remove non-specifically bound peptides. Phosphopeptides were eluted using 20% acetonitrile with 5% ammonium hydroxide and concentrated by vacuum centrifugation.

2.6. Strong cation exchange fractionation

Eluate (45 µL each) from five biological replicates of reversibly oxidized Cys enrichment used in the label-free quantification study was pooled (225 µL total) for fractionation by strong cation exchange (SCX) chromatography using a 60 mg/3.0 mL Supel-Select SCX SPE cartridge (Supelco, Bellefonte, PA). Mobile phase A consisted of 20% acetonitrile with 5 mM ammonium formate, pH 2.7 and mobile phase B was 20% acetonitrile with 500 mM ammonium formate, pH 3. The SCX cartridge was conditioned with 1 mL of methanol and pre-eluted using 1 mL of mobile phase B before equilibration with 1 mL of mobile phase A.

Pooled eluate was dried by vacuum centrifugation and resuspended in 1 mL of mobile phase A before loading onto the equilibrated resin in two passes. The flow-through was collected and peptides were then sequentially eluted from the resin using 1 mL of each elution buffer (in order: 0%, 20%, 40%, 60%, 80%, and 100% mobile phase B in mobile phase A). Remaining peptides were eluted from the resin using 1 mL of 80% acetonitrile with 0.1% TFA. SCX flow-through and fractions were then dried by vacuum centrifugation and desalted by solid-phase extraction before analysis.

2.7. LC-MS/MS analysis

Samples were resuspended in 50 µL of 3% acetonitrile with 0.1% TFA and 5 mM DTT to prevent oxidation of reduced thiols prior to LC-MS/MS analysis. Peptides were analyzed using a NanoAcquity UPLC system (Waters) coupled to a TripleTOF 5600 mass spectrometer (AB Sciex, Framingham, MA, USA). Mobile phase A consisted of water with 0.1% formic acid and mobile phase B was acetonitrile with 0.1% formic acid. Injections (5 µL) were made to a Symmetry C_{18} trap column (100 Å, 5 µm, 180 µm × 20 mm; Waters) with a flow rate of 5 µL/min for 3 min using 99.9% A and 0.1% B. Peptides were then separated on a HSS T3 C_{18} column (100 Å, 1.8 µm, 75 µm × 250 mm; Waters) using a linear gradient of increasing mobile phase B at a flow rate of 300 nL/min. Mobile phase B increased to 35% in 90 min before ramping to 85% in 5 min, where it was held for 5 min before returning to 5% in 2 min and re-equilibrating for 13 min. The mass spectrometer was operated in positive polarity and high sensitivity mode. MS survey scans were accumulated across a *m/z* range of 350–1600 in 250 ms. For information dependent acquisition, the mass spectrometer was set to automatically switch between MS and MS/MS experiments for the first 20 features above 150 counts having + 2 to + 5 charge state. Precursor ions were fragmented using rolling collision energy ± 5% with an accumulation time of 85 ms. Dynamic exclusion for precursor *m/z* was set to an 8 s window. Automatic calibration was performed every 8 h using a tryptic digest of BSA protein standard to maintain high mass accuracy in both MS and MS/MS acquisition.

2.8. Database searching and label-free quantification

Acquired spectral files (*.wiff) were imported into Progenesis QI for Proteomics (Nonlinear Dynamics, version 2.0). A reference spectrum was automatically assigned and total ion chromatograms were then aligned to minimize run-to-run differences in peak retention time. Each sample received a unique factor to normalize all peak abundance values resulting from systematic experimental variation. Alignment was validated (> 80% score) and a combined peak list (*.mgf) for all runs was exported for peptide sequence determination and protein inference by Mascot (Matrix Science, version 2.5.1). Spectral files from SCX fractions were simply converted to peak lists using MS Data Converter (AB Sciex, version 1.3) and merged together. Database searching was performed against a combined database (19,603 entries total) containing *C. reinhardtii* JGI v5.5 proteins (www.phytozome.net; accessed June 2016) and entries from the NCBI chloroplast (BK000554.2) and mitochondrial (NC_001638.1) databases. Sequences for common laboratory contaminants (www.thegpm.org/cRAP; 116 entries) were appended to the database. Searches of MS/MS data used a trypsin protease specificity with the possibility of two missed cleavages, peptide/fragment mass tolerances of 15 ppm/0.1 Da, and variable modifications of acetylation at the protein N-terminus, carbamidomethylation at cysteine, deamidation at asparagine or glutamine, oxidation at methionine, and phosphorylation at serine, threonine, or tyrosine. Significant peptide identifications above the identity or homology threshold were adjusted to less than 1% peptide FDR using the embedded Percolator algorithm [32] and uploaded to Progenesis for peak matching before exporting peptide measurements.

2.9. Data analysis and statistics

Data was parsed using custom scripts written in the Python programming language. Peptides were considered only if Mascot ion score was greater than 13 and normalized abundance was above 0 for at least three replicates within each condition. Shared peptides between proteins were grouped together to satisfy the principle of parsimony and represented by the protein accession with the highest number of unique peptides, else the protein with the largest confidence score assigned by Progenesis. After grouping, site localization of variable modifications was performed using an implementation of the Mascot Delta Score [33]. Localization probability was found using the difference between the best and second best Mascot ion score for alternative modification sites on an otherwise identical peptide-spectrum match. We did not remove any peptides in this step, rather flagged PSMs to suggest additional interrogation by researchers. For redox datasets, results were limited to only peptides with one or more Cys-sites of reversible oxidation, defined here as the absence of carbamidomethylation on at least one cysteine residue in the peptide sequence. For label-free quantification, datasets were reduced to only peptides with unique Cys-site combinations in the protein sequence by summing the abundance of all contributing features (*i.e.*, peptide charge states, missed cleavages, combinations of additional variable modifications). Groups with the same Cys-site identifier were represented by the peptide with the highest Mascot score. Phosphopeptide enriched datasets were parsed similarly, but for unique combinations of phosphorylation sites.

2.10. Functional annotation

Gene ontology (GO) enrichment analysis of protein sequences was performed using KOBAS 3.0 (http://kobas.cbi.pku.edu.cn/) [34] with the following parameters: 'Gene-list Enrichment', *Chlamydomonas reinhardtii* species, GO Slim database, background of all Chlamydomonas proteins, Fisher's exact test with Benjamini and Hochberg multi-test adjustment, and 5 minimum mapping entries. Summarization of GO term redundancy was done using REVIGO [35] (www.revigo.irb.hr) with default parameters except allowed similarity set to small (0.5). Redundant terms were then manually removed from the KOBAS output and visualization/interpretation was performed on the remaining subset.

The entire Chlamydomonas database was annotated with KEGG orthology (KO) identifiers using KAAS (http://www.genome.jp/tools/kaas) [36], where the BLAST program searched *A. thaliana* and *C. reinhardtii* reference genes applying a bi-directional best hit default threshold. Pathway reconstruction for protein lists was then performed using the KEGG Mapper (http://www.genome.jp/kegg/tool/map_pathway.html) [37] with KO identifiers supplied by KAAS. Pathways maps were then binned together into respective modules to better summarize annotations. Pathways featured in maps for both global/overview and organismal systems were removed from consideration for being excessively broad in definition.

2.11. Motif analysis

Each reversibly oxidized Cys-site measured with label-free quantification (3353 sites) was mapped to the corresponding protein and the five neighboring residues toward both protein termini were recorded, generating a 20 residue x 10 position matrix. Sites too close to protein termini to properly extend the residue window were excluded from analysis (3308 remaining). This procedure was repeated for all Cys in the proteome (191175 sites) to generate another matrix containing the background distribution. The count for each unique combination of neighboring residue and position was divided by the corresponding background to generate a position weight matrix containing the relative frequency as a percentage of the background. The matrix was displayed as a heatmap colored using a gradient from white to blue for the minimum and maximum relative frequency, respectively.

2.12. Comparison to previously identified modifications

Proteins with sites of reversible oxidation were compared with literature [19–21] by BLAST searching (blastp, version 2.7.1) [38] to the Chlamydomonas UniProtKB database (www.uniprot.org/proteomes/UP000006906; accessed October 2016). Each Chlamydomonas protein in the Phytozome database was searched using default parameters with an E-value cutoff of 0.001 and selection of the top ranking hit. Some literature annotations were converted (*i.e.,* from 'NCBI RefSeq' to 'UniProtKB AC/ID') using the 'Retrieve/ID mapping' tool (www.uniprot.org/uploadlists/). When discussing site-specificity, the associated UniProt protein ID and provided Cys-site were concatenated to generate an 'Identifier' handle used for comparisons.

2.13. Data availability

The mass spectrometry proteomics data have been deposited to the ProteomeXchange Consortium (www.proteomexchange.org) via the PRIDE partner repository [39] using identifiers PXD008370 for initial optimization of sequential enrichment, PXD008371 for label-free quantification, and PXD009038 for SCX fractionation PXD009038.

3. Results and discussion

3.1. Enriching the redox thiol proteome with sequential phosphorylation analysis

Identification and site-specific quantification of reversible thiol oxidation has been readily performed *via* differential alkylation-based methods utilizing thiol-disulfide exchange chromatography [40,41] that have been tailored for specific modifications including *S*-nitrosylation [42,43], *S*-glutathionylation [44,45], and *S*-acylation [46]. Here we applied this strategy for quantitative profiling of reversible oxidation on intact Chlamydomonas proteins (Fig. 1A). The *in vivo* redox status of protein cysteines was quenched by performing cell lysis under denaturing conditions in the presence of IAM to block reduced thiols [47], which we have previously shown to be rapid and efficient in alkylation [22]. Artifactual oxidation by Fenton-derived free radicals was prevented with the addition of DTPA metal chelator [48] and unnecessary reduction of *S*-nitrosothiols was avoided by selective Cu(I) chelation using neocuproine [49]. All reversibly oxidized Cys-residues were then reduced using DTT and nascent thiols enriched at the protein-level using Thiopropyl Sepharose 6B (TPS6B) resin for thiol-disulfide exchange chromatography [41]. On-resin trypsin digestion of Cys-bound proteins was performed and unbound peptides collected for subsequent phosphopeptide enrichment. Cys-bound peptides were then eluted from the resin using DTT and subjected to LC-MS/MS analysis to survey reversibly oxidized sites.

Phosphorylation of redox-modified proteins was surveyed using a sequential enrichment approach (Fig. 1B), where initially proteins were bound to TPS6B resin and the unbound proteome washed away. Trypsin protease was then added for on-resin digestion and unbound peptides were collect in the flow-through. The resin was washed and bound Cys-peptides then eluted using DTT reductant. Peptides collected in both the eluate and flow-through represent fragments of proteins previously bound by a Cys-site of reversible oxidation. Eluate and flow-through were then combined before enriching for phosphopeptides with TiO$_2$ resin [26] and using LC-MS/MS analysis to determine the extent of phosphorylation in the redox proteome. Since eluate and flow-through were collected separately, it was possible to remove a small portion of the eluate for analysis of redox Cys-peptides without phosphopeptide enrichment. The remaining eluate was combined with an equal proportion of flow-through and taken through sequential phosphopeptide enrichment. In this way, a single sample could be used for analysis of both the redox proteome and phosphorylated subset.

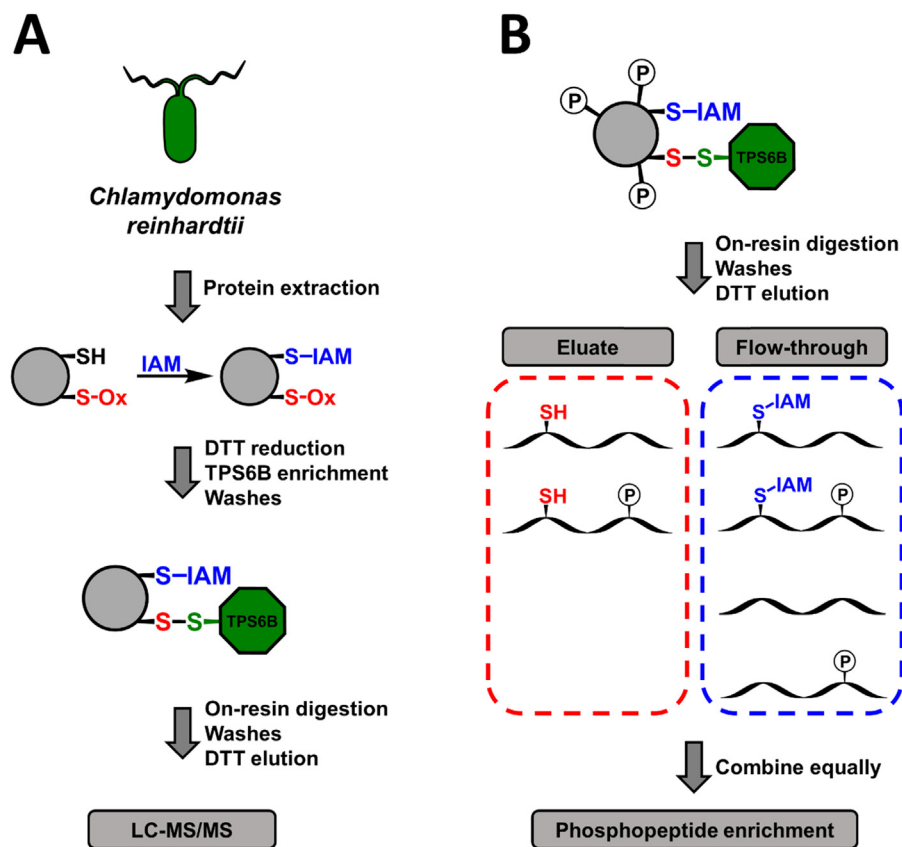Initially one biological replicate of Chlamydomonas was taken

Fig. 1. Workflow schematic for differential alkylation-based enrichment of redox proteins. (A) Proteins were extracted from Chlamydomonas cells and *in vivo* reduced Cys alkylated with IAM before DTT reduction of oxidized Cys and capture of nascent thiols using TPS6B resin at the protein-level. For LC-MS/MS analysis, bound proteins were digested with trypsin and the eluate collected. (B) Sequential enrichment of phosphopeptides after on-resin digestion and stoichiometric recombination of peptide eluate and flow-through.

through redox Cys profiling and sequential enrichment of phosphorylation. Upon enrichment of proteins with reversibly oxidized Cys and on-resin digestion, peptide samples from the unbound flow-through and Cys-bound eluate were collected separately. Of the 3542 distinct peptides identified in the eluate, the majority (3329) had sites of reversible Cys oxidation spread across 1335 proteins (Fig. 2A; Supplemental Table S1). The flow-through featured an increased protein count (1657) composed mostly of peptides lacking Cys residues (7505) or those with alkylated Cys only (1045), which was promising since these peptides were not expected to bind to the resin following proteolytic digestion of Cys-bound proteins (Supplemental Table S2). Just 30 peptides with oxidized Cys were identified in the flow-through, highlighting the efficiency of TPS6B resin at capturing and retaining only reduced thiols (*i.e.*, previously oxidized Cys reduced with DTT).

Nearly 63% of redox proteins found in the eluate were also identified in the flow-through following on-resin digestion (Fig. 2B). While in theory this overlap should be complete, it accurately reflects that proteins are considered to produce multiple peptides following trypsin digestion, where some can be too small/large or not basic enough for identification by LC-MS/MS analysis [50]. This can be for redox Cys-containing peptides in the eluate or general peptides in the flow-through such that if a protein is digested and produces an undetectable redox Cys-peptide and a detectable peptide, then the result would be that the protein is only identified in the flow-through. Further hindering bottom-up proteomics, current LC-MS/MS methods rarely identify every peptide in a particular sample because of: (1) the stochastic nature of LC-MS/MS using data-dependent acquisition strategies, (2) poor MS/MS fragmentation of certain peptides, and (3) insufficient separation using reversed-phase LC [51]. Given the binding specificity for only redox-modified Cys shown in Fig. 2A, the unique subset of proteins identified in Fig. 2B can thusly be considered new components of the redox proteome, where each protein was modified with reversible oxidation at a particular Cys-site not detected in the study, but hypothesized to exist in order for the protein to have

originally bound to the resin. Additionally, of the 818 proteins identified uniquely in the flow-through, 106 did not contain a Cys in the protein sequence and were considered either: (1) low abundance contaminants that were not removed during resin washing or (2) artifacts of database searching and protein inference between samples with unique peptide subsets (*i.e.*, eluate and flow-through). Nevertheless, our analysis of eluate and flow-through showed the latter having more sequence information for bound proteins. This is consistent with the observation that Cys have a relatively low frequency of ~1% across the Chlamydomonas proteome (Fig. S1A) with reversible oxidation occupying only an estimated 10% of Cys under normal growth conditions [52], leaving the majority of tryptic peptides (even those bearing Cys residues) unbound after on-resin digestion.

The remaining eluate, flow-through, or an equal combination thereof were used to benchmark the coverage obtainable from sequential enrichment of phosphorylation. An equal combination of eluate and flow-through was used to mimic the stoichiometry achieved from a typical in-solution digestion. The eluate identified considerably less phosphoproteins (63) compared to flow-through (651), while the combined sample had the most phosphoproteins (697) and shared a majority with flow-through (Fig. 2C; Supplemental Tables S3-S5). Although our approach broadly identified phosphopeptides from redox proteins, distinguishing which modifications occurred on the same proteoform following proteolytic digestion was restricted to detecting co-modified peptides. As the eluate contained primarily redox peptides, it expectedly had the deepest coverage of phosphopeptides with oxidized Cys sites (Fig. 2D). A majority of proteins in Chlamydomonas (86%) contain more than one Cys residue (Supplemental Fig. S1B) and may possess both reduced and oxidized sites *in vivo*. This observation is supported in the flow-through identifying largely phosphopeptides with only reduced Cys (*i.e.*, alkylation at Cys), where the three detected in eluate are considered non-specific peptides remaining after on-resin digestion and washes. The combined sample had relatively high coverage for both types of doubly-modified phosphopeptides, so all
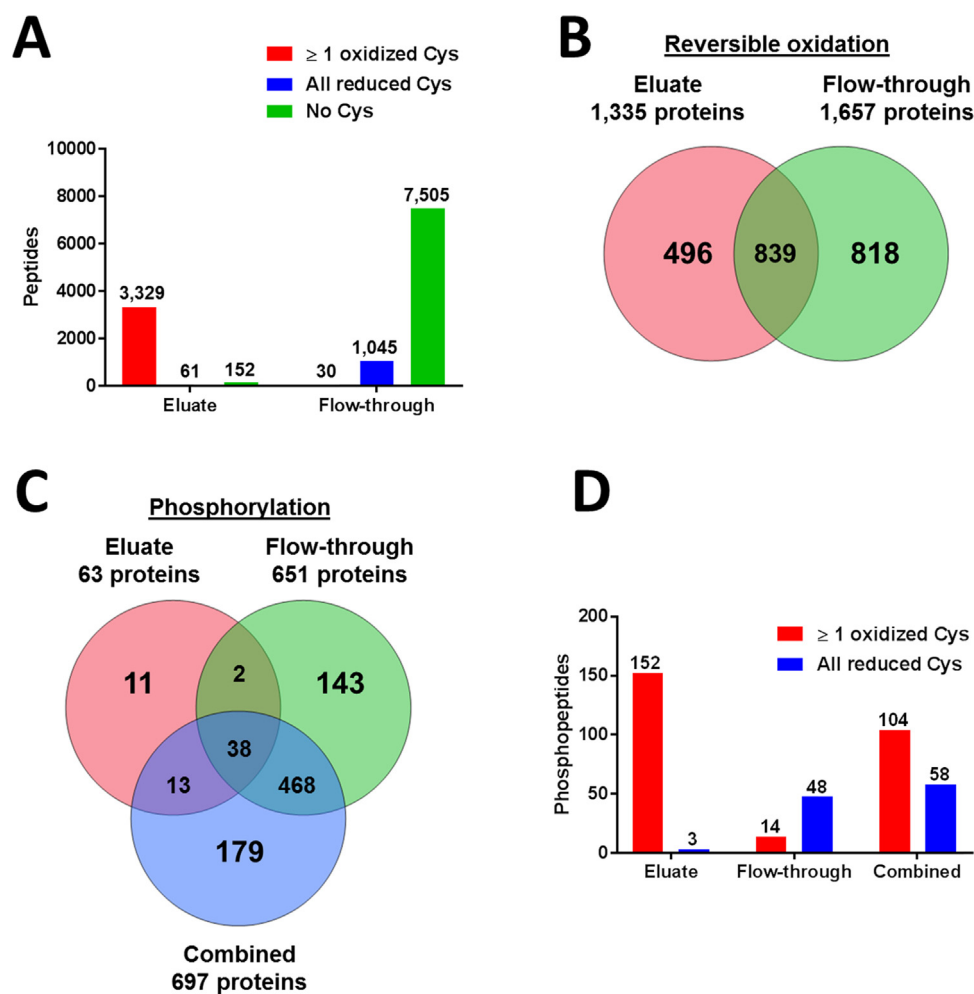
Fig. 2. Optimization of redox and sequential phosphopeptide enrichment. (A) Distribution of peptide types identified in either eluate or flow-through. (B) Protein coverage obtained from distinct portions from redox enrichment. (C) Overlap of phosphoproteins identified from sequential phosphopeptide enrichment of distinct portions from redox enrichment. (D) Distribution of Cys-phosphopeptides identified with either reduced or oxidized Cys-sites from each sequential enrichment type.

subsequent experiments followed this approach. It is noteworthy to mention that using only eluate in phosphopeptide enrichment reflects methods used in various mammalian cell lines with considerable success [27,28] and will determine the largest number of doubly-modified redox proteoforms by identifying mostly peptides with both oxidized Cys and phosphorylation.

3.2. Coverage and reproducibility of sequential enrichment using label-free quantification

To determine the precision of our sequential enrichment method and explore the dynamic range of PTM abundance, we employed label-free quantification (LFQ) of peptide peak areas [53] across five biological replicates to measure 4780 redox peptides in the eluate, summarizing to 3251 peptides with distinct oxidized Cys-sites from 1490 proteins (Supplemental Table S6). The efficiency of enrichment, defined as the ratio of redox peptides to the total number of peptides quantified after the DTT elution step, was 92% and indicated high specificity of the method for binding cysteine thiols only. Despite removing excess DTT using filtration devices with a 10 kDa cutoff, there were 18 identified proteins with molecular weights below 10 kDa in the dataset. Proteins were denatured with urea and SDS prior to buffer exchange, which increased their Stokes radii and largely prevented passage through the filter [54], thereby allowing low molecular weight proteins to be retained and analyzed subsequently. Overall coverage was slightly decreased when comparing protein-level enrichment in this study to our

previous work enriching redox peptides following trypsin digestion (3662 redox peptides from 1924 proteins) [22], however the method used for protein extraction in this study incorporated an increased IAM incubation period (2 h instead of 15 min) to improve alkylation efficiency and lower the potential for falsely identifying oxidized Cys. We did not observe significant differences in coverage between peptide- and protein-level enrichments when using lysate from identical extraction procedures (data not shown). To further validate the protein-level dataset and demonstrate that alkylation was sufficiently complete, redox peptides were culled by ~5% after removing Cys-sites also identified in a negative control where DTT reduction was omitted prior to enrichment. The remaining 3094 peptides confidently defined 3353 oxidized Cys-sites from 1457 proteins. Redox enrichment at the protein-level showed high reproducibility with a median coefficient of variation (CV) of 22% across biological replicates.

Sequential enrichment of phosphopeptides was performed for each biological replicate used in the redox LFQ experiment. Samples were prepared by dividing both the eluate and flow-through in half. One portion of eluate was directly processed for redox Cys profiling, while the other was combined with one half of the flow-through to represent equal stoichiometry (*i.e.*, representative of the stoichiometry achieved from a typical in-solution digestion). We quantified 1099 peptides with distinct phosphorylation sites from 740 proteins. Twenty contaminant proteins were removed with an additional filter that all phosphoproteins must contain at least one cysteine in the protein sequence. The resulting phosphorylated redox proteome thusly amounted to 1065
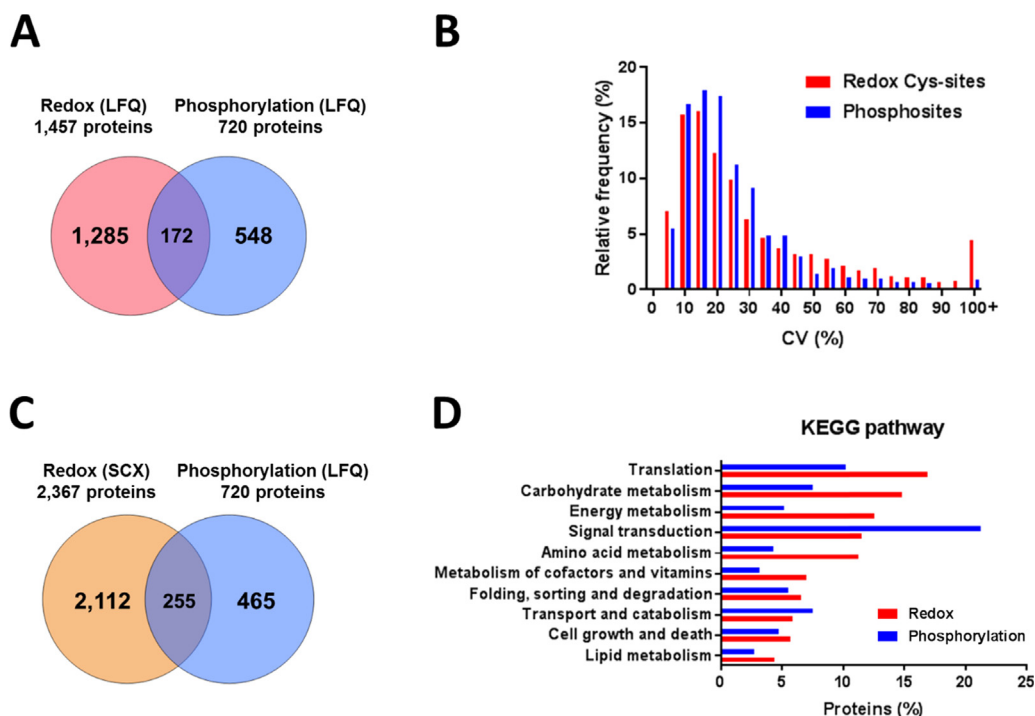
Fig. 3. Coverage and reproducibility of redox Cys-sites and sequential phosphopeptide enrichment. (A) Overlap of proteins identified from redox and sequential phosphopeptide enrichment. (B) Histogram of the coefficient of variation (CV) as a percentage for all redox Cys and phosphosites quantified. (C) Comparison of proteins identified from SCX fractionation of redox Cys eluate to phosphoproteins in the LFQ dataset. (D) Functional pathway classification of redox and phosphorylated proteins in the LFQ datasets. The Y-axis indicates the KEGG pathway and the X-axis represents the percentage of annotated redox (703 total) or phosphorylated redox (254) proteins assigned to a particular category.

phosphopeptides, distributed as 1094 unique sites on 720 proteins (Supplemental Table S7). Half of these phosphosites (554) were found localized on peptides in another study defining the global Chlamydomonas phosphoproteome [25], providing additional validation for phosphosite validity. Although phosphopeptides were solely enriched from a tryptic digest of redox proteoforms, only 172 (23%) identified phosphoproteins were shared with the reversibly oxidized proteome (Fig. 3A). The 548 uniquely identified phosphoproteins must all contain at least one reversibly oxidized cysteine to have bound to the TPS6B resin, serving as an expanded database of previously undetectable redox proteoforms using the LFQ pipeline. Notably, 37 of these phosphoproteins contained only one Cys residue in the protein sequence, which are therefore considered to be sites of *in vivo* reversible oxidation. The additional enrichment of phosphopeptides did not introduce excessive variation, where median CV was 20% across replicates (Fig. 3B).

To examine the low overlap between redox proteins and, presumably inclusive, phosphorylated redox proteins, we compared the dynamic ranges of modification sites supplied by label-free quantification to determine if any underlying biases were present. Each unique redox Cys-site identifier was represented by the mean abundance across biological replicates and partitioned by whether or not the corresponding protein was shared with or unique to phosphorylated redox proteins (Supplemental Fig. S2A). A normal distribution was observed for redox Cys-sites with similar means regardless of whether proteins were found to also be phosphorylated. Complementary analysis of phosphosite identifiers that were either shared with or unique to redox proteins (Supplemental Fig. S2B) revealed separated distributions, where phosphosites on proteins shared with redox were generally higher abundance than those found on uncommon proteins by nearly one order of magnitude. The majority of phosphoproteins in our dataset are likely low abundance proteoforms that preclude detection without phosphopeptide enrichment, as many groups have previously concluded [55,56]. Overcoming this abundance disparity from phosphopeptide enrichment would therefore require improved coverage of the redox proteome to push the limit of detection increasingly lower and enable identification of the remaining proteins found only to be phosphorylated.

We next examined whether the low overlap between proteins identified in redox and phosphorylated redox datasets was simply an analytical challenge, and not an underlying feature of reversible oxidation, by fractionating redox Cys eluate with strong cation exchange (SCX) chromatography. This allowed superior coverage of the redox proteome, identifying 6973 distinct peptides with previously oxidized Cys across 2402 proteins (Supplemental Table S8). To reduce false positive identification of oxidized Cys, 35 proteins were removed that had all of their Cys-sites also found in the negative control enrichment used in the LFQ experiment. There remained 6642 redox Cys-peptides from 2367 proteins, of which 1248 proteins (86%) in the redox LFQ dataset were shared (Supplemental Fig. S3A). Importantly, there were 255 proteins identified in both the fractionated redox proteome and phosphorylated redox LFQ dataset (35%), improving the phosphoprotein overlap by 12% compared to the unfractionated redox LFQ dataset (Fig. 3C). While continued fractionation of the redox eluate should achieve complete overlap with identified phosphoproteins, the peptide flow-through from redox enrichment still contained a large subset of proteins not found in fractionated redox eluate (Supplemental Fig. S3B). This lack of overlap suggests a fundamental limitation for the identification of certain proteins using redox Cys-peptides alone.

Many peptides found from redox enrichment contained only a single redox Cys-site (83%), whereas 96% of phosphopeptides had a single phosphosite (Supplemental Fig. S4A). The latter finding is consistent with TiO_2-based enrichment favoring singly phosphorylated peptides [57]. Most phosphorylation events (83%) were detected on serine residues, followed by 15% on Thr and only 2% on Tyr, comparable to previous phosphosite distributions reported in Chlamydomonas [25,26]. We next looked at how many unique sites occurred per protein and found that redox modifications tend to be more numerous than phosphorylation (Supplemental Fig. S4B), likely due to the enrichment of structural, intramolecular disulfide bonds highly abundant in the redox proteome under normal growing conditions [58]. Interestingly, relative to the background Chlamydomonas proteome, a large proportion of redox Cys found in this study had neighboring lysine residues in the protein sequence (Supplemental Fig. S4). It has been similarly reported in humans that lysine-rich motifs are enriched around redox-active Cys residues [59] and that these lysine may act as hydrogen donors to stabilize thiolate anions, thereby reducing the pK_a of adjacent

Cys and potentially increasing thiolate reactivity at physiological pH [60]. Additionally, both ubiquitination [61] and carbonylation [62,63] of lysine are recognized hallmarks of oxidative stress response and likely co-occur with thiol oxidation on many proteins [64].

3.3. Comparison to previously identified modifications

This work featured enrichment of the entire proteome with reversibly oxidized Cys using DTT reductant, regardless of the particular redox PTM type. Previous studies in Chlamydomonas have targeted specific redox modifications on proteins, such as *S*-glutathionylation [19], *S*-nitrosylation [20], and TRX-dependent reduction [21]. We compared which proteins in our redox LFQ dataset were experimentally identified in these publications, finding 535 TRX-reduced, 244 nitrosylated, and 129 glutathionylated proteins (Supplemental Table S6). Likewise in our phosphorylated LFQ dataset, there were 126 TRX-reduced, 52 nitrosylated, and 29 glutathionylated proteins (Supplemental Table S7). We additionally parsed the phosphorylated LFQ dataset for the 548 phosphoproteins identified from sequential enrichment that were not found in the redox LFQ data (Fig. 3A), revealing 46 proteins as TRX-targeted, 10 nitrosylated, and 5 glutathionylated, thereby validating their presence in the phosphorylated redox proteome. Regarding site-specific overlap, our redox LFQ dataset (3353 Cys-sites) contained 267 Cys previously identified as TRX-targeted, 106 nitrosylated, and 19 glutathionylated (Supplemental Table S9). While BLAST searching resulted in finding homologous accessions between the Phytozome and UniProt databases, there existed differences in the exact position of Cys residues between many sequence pairs, ultimately leading to an underestimation of previously identified sites of Cys oxidation. However, even with complete overlap, out study used

Similar comparisons were made for phosphorylation using data from previous work that localized 15,862 phosphosites on 4588 proteins to define the global Chlamydomonas phosphoproteome [25]. Phosphoproteins identified from sequential enrichment of the redox proteome had 442 proteins also found in the global Chlamydomonas phosphoproteome (Supplemental Table S7), where at the individual phosphosite-level, the phosphorylated LFQ dataset had 556 sites (51% of 1094 total) that were previously localized (Supplemental Table S10). There were 446 proteins in the redox LFQ dataset previously identified as phosphorylated (Supplemental Table S6), suggesting that the maximum extent of expected phosphorylation in the redox proteome was 31% of the 1457 oxidized proteins identified. However, this comparison only revealed the proportion of known targets for both PTMs and does not specify the theoretical maximum of doubly-modified proteoforms, which is uniquely shown by this study using a sequential enrichment strategy for phosphorylation of the redox proteome.

3.4. Proteoform inference

Clear identification of proteoforms was achieved by sequencing doubly-modified peptides, as the co-occurrence of these modifications can be inferred back to a portion of the intact protein before digestion. With no enrichment for phosphorylation, only 9 peptides detected from 8 proteins had both an oxidized Cys and phosphorylation site. Using sequential enrichment, we observed 75 Cys-containing phosphopeptides from 59 proteins (Supplemental Table S11). Twenty-eight of these peptides had at least one oxidized Cys-site in the sequence, expanding the redox proteome by 14 proteins not identified from redox enrichment alone. The remaining 47 phosphopeptides with only reduced Cys (*i.e.*, identification of alkylation at the Cys residue) did not have free Cys available for enrichment with TPS6B resin. This subset of reduced Cys-phosphopeptides must have been from the flow-through and originated from proteoforms with at least another Cys residue in the protein sequence that was reversibly oxidized. Using this approach, it was possible to fit 17 proteins into this modification clique by having an identified peptide with both reduced Cys and phosphorylation and also

having an oxidized peptide on distant Cys identified in the redox dataset. For example, small subunit ribosomal protein S13e (RPS13; Cre07.g331900.t1.2) is a structural component of the ribosome necessary for proper translation of proteins and is 151 amino acids in length with only two Cys (C26 and C38) in the sequence. This protein was previously identified as phosphorylated at S21 [25], which we quantified in this study as '(pS)PPSW(redC)K' in phosphorylated redox (Supplemental Table S7), both singly phosphorylated (S21) with a reduced Cys (C26). This same peptide was quantified in redox (Supplemental Table S6) as 'SPPSW(oxC)K′ and was oxidized at C26 without phosphorylation at S21. The redox LFQ dataset also measured a longer form of this peptide 'SPPSW(oxC)KTTGAEVQEMI(oxC)K' with oxidation occurring at both C26 and C38. Moreover, the sequential phosphopeptide enrichment of only the redox eluate (Supplemental Table S3) identified '(pS)PPSW(oxC)K' with phosphorylation at S21 in addition to oxidation at C26. Taken together, these results suggest RPS13 existed in several forms: (1) a fully oxidized proteoform of RPS13 without phosphorylation on S21, (2) a phosphorylated form reduced at C26 and hypothetically oxidized at C38 (necessary for the proteoform to bind to the TPS6B resin), and (3) a phosphorylated form oxidized at C26 with an unknown status of C38.

3.5. Pathway annotation

We classified proteins according to KEGG pathways to find major biological features in both the redox and phosphorylated redox proteomes (Fig. 3D). Of the 703 redox proteins annotated, most were attributed to either 'translation' (17%), 'carbohydrate metabolism' (15%), or 'energy metabolism' (13%). The 254 annotated phosphoproteins were from primarily 'signal transduction' (21%), 'translation' (10%), and 'transport and catabolism' (7%). Redox proteins showed a noticeably larger proportion of proteins in 'amino acid metabolism' (2.6-fold), 'energy metabolism' (2.4-fold), and 'metabolism of cofactors and vitamins' (2.2-fold), while phosphoproteins were most differential in the 'signal transduction' pathway (1.8-fold). Similar pathways were overrepresented for each by gene ontology enrichment analysis, where biological processes for redox were mainly involved with metabolism and phosphorylated redox featured signal transduction and protein phosphorylation (Supplemental Fig. S5). The KEGG pathways most populated for the 77 annotated out of 172 shared proteins between the enrichment methods were 'signal transduction' (29%), 'translation' (17%), and 'carbohydrate metabolism' (16%).

3.6. Translation

Structural constituents of the 'ribosome' (KO03010) were found highly modified by oxidation (126 unique redox Cys on 67 proteins) and phosphorylation (14 phosphosites on 9 proteins), with 7 ribosomal subunits affected by both modifications. There were 30 redox proteins and 11 phosphoproteins, including 5 also found oxidized, that are considered part of 'RNA transport' (KO03013) or 'mRNA surveillance pathway' (KO03015). PTMs serve as a conditional adjustment of protein biosynthesis and turnover necessary for environmental acclimation [65] and the identification of dually-modified components of translational machinery may reveal additional mechanisms to fine-tune activity [66].

3.7. Energy metabolism

Reversible oxidation of proteins involved with energy metabolism was considerable (13% of 703 redox proteins annotated onto KEGG pathways), where 33 proteins were from 'oxidative phosphorylation' (KO00190) and 20 proteins mapped to either 'photosynthesis' (KO00195) or 'photosynthesis – antenna proteins' (KO00196). Photosynthesis is a process of photochemical energy transduction that is constantly optimized in changing light conditions by balancing the
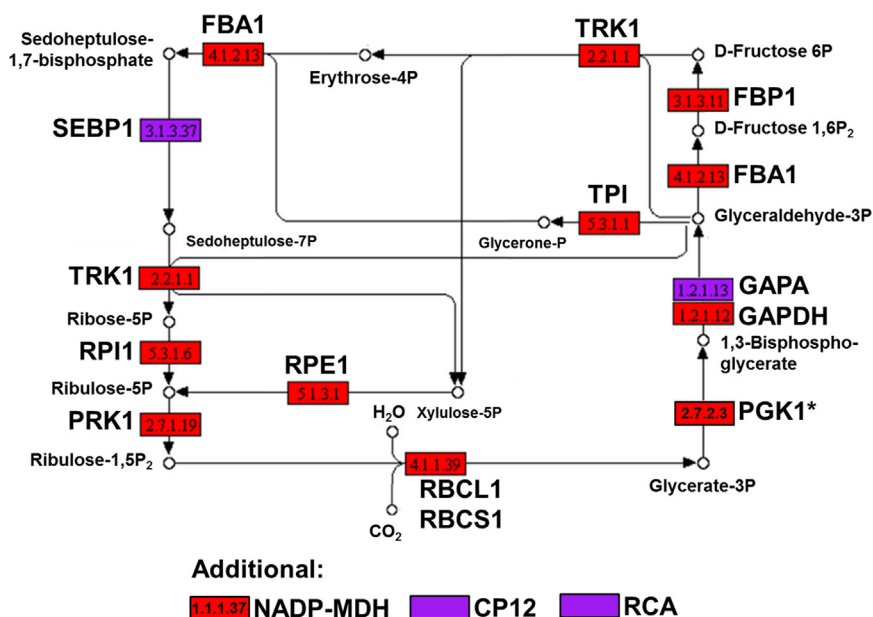
Fig. 4. Representative coverage of Calvin-Benson cycle enzyme. KEGG pathway map adapted for the 'Calvin-Benson cycle' module of 'Carbon fixation in photosynthetic organisms' (www.genome.jp/dbget-bin/www_bget?cre00710). Boxes represent proteins in the pathway and are labeled with Enzyme Nomenclature numbers. Proteins are colored according to modifications found in this study: red for redox coverage only and purple for identification of both redox and phosphorylation sites. Proteins are abbreviated by either UniProt or KEGG gene names. An asterisk (*) marked PGK1 to show that it was identified with reversible oxidation in the preliminary experiment, but not in the LFQ datasets.

amount of light absorbed by photosystems I and II [67]. Dephosphorylation of light-harvesting complex II by thylakoid-associated phosphatase 38 (TAP38; Cre04.g218150.t1.2) is necessary for fast phospho-signaling in state transitions of *A. thaliana* [68,69] and this protein was quantified in this study only with reversible oxidation at two Cys (C135 and C282), but known to be phosphorylated at T138 and T171 [25], suggesting distinct proteoforms may exist with variable phosphatase activity. Chloroplast-localized serine/threonine-protein kinase STT7 (Cre02.g120250.t2.1) and STL1 (Cre12.g483650.t1.2) were also found with sites of reversible oxidation and phosphorylation in this study.

The 'carbon fixation in photosynthetic organisms' (KO00710) pathway was well-represented, particularly in the Calvin-Benson cycle (CBC), where all proteins were identified with reversible oxidation and four were additionally phosphorylated (Fig. 4). Phosphoglycerate kinase (PGK1; Cre11.g467770.t1.1) was not found in either LFQ dataset, but was identified reversibly oxidized at C159, C278, and C412 in the preliminary experiment (Supplemental Table S1). Nevertheless, PGK1 in Chlamydomonas is known to undergo TRX-dependent activation in the light by reduction of a regulatory disulfide bond between C-terminal C278 and C412 [70] and has been identified before with *S*-glutathionylation at C159 [19]. Previous reports in Chlamydomonas have moreover shown that all CBC proteins undergo TRX-dependent reduction [71] with additionally observed sites of nitrosylation and glutathionylation at key Cys residues [5,20]. In addition to reversible oxidation, our results demonstrated that four CBC proteins were also phosphorylated: sedoheptulose-bisphosphatase (SEBP1; Cre03.g185-550.t1.2), chloroplastic glyceraldehyde 3-phosphate dehydrogenase (GAPA; Cre01.g010900.t1.2), rubisco activase (RCA; Cre04.g 229300.t1.1), and CP12 domain-containing protein 1 (CP12; Cre08.g380250.t1.2).

SEBP1 contains seven Cys residues that were all measured with reversible oxidation in this study, with *S*-nitrosylation previously detected on C-terminal C351 and C358 residues [20]. Additionally, C111 and C116 mimic C52 and C57 in the wheat homolog, which have been shown to form a regulatory disulfide bond that potentially modulates protein activity [72]. We identified three phosphosites (S110, T114, and S119) in close proximity to the suspected C111-C116 disulfide bond, suggesting an additional layer of control to SEBP1 activity.

In green algae, chloroplastic GAPDH is encoded only by the A subunit (GAPA) and lacks the specific C-terminal extension found on the GAPB subunits of higher plants, which harbors a pair of Cys residues

targeted by TRX for light/dark enzymatic regulation [73]. In our redox LFQ dataset, GAPA was reversibly oxidized on C190 and C194, where the former Cys has previously been identified as a site of *S*-glutathionylation in Chlamydomonas [19]. We additionally quantified phosphorylation on T87 of GAPA, however the functional implication of this modification is questionable as identified phosphosites on this enzyme significantly differ in location between photosynthetic organisms [74].

RCA is a member of the AAA(+) family of molecular chaperones and releases inhibiting sugar phosphates from the catalytic site of Rubisco, thereby impacting the overall yield of the carbon assimilation cycle [75]. Only the shorter RCAβ isoform is expressed in Chlamydomonas and exhibits redox regulation despite lacking the regulatory C-terminal disulfide found in the RCAα isoform of many plant species [76,77]. The four Cys residues found in Chlamydomonas RCA (C148, C196, C255, and C289) have all been previously identified as TRX-reduced [21], where C196 has additionally been found *S*-nitrosylated [20] and RCA generally identified as a target of glutathionylation [19]. Moreover, RCA is known to be phosphorylated at ten positions [25], where S53 phosphorylation is known to be catalyzed by the thylakoid-localized STT7 kinase and has been suggested to increase RCA attachment to the thylakoid membrane and protect STT7 from proteolysis [78]. In this work, we quantified three sites of reversible oxidation on RCA (C148, C196, and C255) and two sites of phosphorylation (S45, S86), perhaps identifying novel aspects of RCA regulation through the concurrent occupation of both PTMs, which has been of considerable interest lately [15].

Another important result from this study was the overall coverage on CP12, which is known to be localized in the chloroplast acting as a linker in the core complex of CBC proteins phosphoribulokinase (PRK) and glyceraldehyde-3-phosphate dehydrogenase (GAPDH), thereby coordinating the reversible inactivation of these proteins [79]. CP12 has four conserved Cys residues and is fully oxidized in the dark by two disulfide bonds (C74-C82 and C117-C126) to allow complexation and direct inactivation of GAPDH, which the binary complex CP12/GAPDH then binds and thereby inactivates PRK [80]. CP12 was highly abundant in our redox enrichment (six identifiers spanning 10^3–10^6 abundance) and confirmed oxidation on all four Cys residues, despite harvesting Chlamydomonas cultures 2 h into the light phase. Phosphorylation of CP12 was also measured (three identifiers with 10^2–10^3 abundance) and identified several peptides including 'GTSAD (redC)AVAWD(pT)VEELSAAVSHK' with both reduced C82 and phosphorylated T88. Another version of this peptide sequence was found

oxidized at C82 with phosphorylation at S79. Near the C-terminal disulfide bond, the peptide 'ADV(pT)LTDPLEAF(oxC)K' showed phosphorylation at T108 close to an oxidized C117. Considering that CP12 is intrinsically unstructured without disulfide bond formation and must form them for proper coordination with GAPDH and PRK [81], it is possible that phosphorylation of these regions additionally changes CP12 conformation to modulate the degree of CP12/GAPDH/PRK complexation. Considering that an additional three phosphosites (S52, T78, and T110) were previously identified [25], there is strong evidence that this protein is affected by both PTMs.

3.8. Signal transduction

Phosphorylation of proteins involved in signal transduction were highest for the 'AMPK signaling pathway' (K04152; 6 entries), 'PI3K-Akt signaling pathway' (K04151; 5 entries), mTOR signaling pathway' (K04150; 4 entries), and 'phosphatidylinositol signaling system' (K04070; 4 entries). A highly phosphorylated protein in this study was inositol hexakisphosphate kinase (VIP1; Cre03.g185500.t1.1) with nine phosphosites and one reversibly oxidized Cys site (C289). VIP1 is known as an inositol hexakisphosphate/diphosphoinositol-pentakisphosphate kinase involved in phosphatidylinositol signaling, which has recently been reported to shown synergism with TOR kinase signaling governing carbon metabolism and lipid accumulation in Chlamydomonas [82]. We identified novel reversible oxidation at C289 on VIP1 within the 'ATP-grasp' domain necessary for inositol diphosphate kinase activity [83].

Reports have indicated the significance behind studying redox effects of phosphorylation-dependent signaling pathways in Chlamydomonas, particularly in TOR kinase signaling [84]. It has long been suggested that redox modifications to key proteins are involved in stress–response TOR signaling [85], with a specific role in regulating the rapamycin-sensitive TOR complex 1 (TORC1) [86], which is conserved in Chlamydomonas [87,88]. Homology to known downstream targets of the TOR kinase, including ribosomal protein S6 kinase beta (RPS6KB; Cre13.g579200.t1.2), can be used to further understand the role of redox signaling on the TOR complex in Chlamydomonas. We identified two RPS6KB peptides spanning the catalytic domain, one phosphorylated at S773 and another both phosphorylated (S915) and with a reduced Cys (C917). The direct target of RPS6KB kinase activity is the small subunit ribosomal protein S6e (RPS6; Cre09.g400650.t1.2), which was identified in this study *via* a redox peptide with one oxidized Cys (C102) and three phosphopeptides (T127, S231, and S245).

Proteins related to autophagy were well represented in this study. For instance, the direct phosphorylation of ULK1 by AMPK is shown to regulate autophagy in mammals [89] and has evolutionary conservation with autophagy-related proteins (ATG) in photosynthetic eukaryotes, suggesting that similar regulatory mechanisms exist in Chlamydomonas. Our data showed quantitative coverage of S803 of ATG1 (Cre09.g391245.t1.1), an essential Ser/Thr kinase involved in autophagy [90], and oxidation of C255 on ubiquitin-like-conjugating enzyme (ATG3; Cre02.g102350.t1.2). Oxidation on ATG3 is within the catalytic domain on the HPC motif necessary for recognition of the ATG5 (Cre14.g630907.t1.1, not detected) subunit of the autophagosome complex [91].

Regarding osmotic stress response, previous reports have found protein phosphatase 2C (PP2C) as a regulator of necessary signal transduction events for development in plants [92] and previously found to be phosphorylated [93]. Two PP2C homologs (Cre03.g211073.t1.1 and Cre02.g141250.t1.2) were identified in the phosphorylated redoxome with five (S4, T18, S61, S63, and S161) and one (S468) site of phosphorylation, respectively. One accession of PP2C (Cre03.g211073.t1.1) was found with triply-modified on the peptide 'QS(pS)A(oxC)LGATGS(oxC)PAHGVK' with two oxidized Cys (C163 and C170) and a phosphosite (S161), revealing that there are PP2C proteoforms with regions occupied by both redox and phosphorylation

events. PP2C acts as a negative regulator of stress-induced MAPK pathways in higher plants [94] and has been shown to inactivate SNF1-related protein kinase (SNRK2) *via* dephosphorylation [95]. Two identified proteins were annotated as SNRK2s (Cre06.g292700.t1.2 and Cre12.g499500.t1.1) and were found to be phosphorylated at S167 and T177, respectively. SNRK2 has been shown to respond in sulfur limitation [96], whereby understanding the significance of both modifications on PP2C and SNRK2s in response to abiotic stress could reveal novel means of stress response in algae.

In summary, we provide an approach to readily detect new targets of both reversible oxidation and phosphorylation using a novel combination of protein-level redox enrichment and subsequent phosphopeptide analysis. This technique was used to (1) define the reversibly oxidized proteome and (2) identify the subset of redox proteins also phosphorylated. Many proteins identified with both modifications in Chlamydomonas were involved in pathways related to signal transduction, translation, and carbohydrate/energy metabolism, suggesting that the co-occurrence of phosphorylation and reversible oxidation provides an underappreciated mechanism for protein regulation. The paradigm that cellular processes are controlled by a single PTM was disputed, notably by several redox-regulated CBC proteins found additionally phosphorylated and that many kinases/phosphatases involved in photosynthetic state transition and stress-response pathways had sites of reversible oxidation. Identification of redox proteins serves as a crucial element in understanding stress response and adaptation in photosynthetic organisms and beyond, whereby knowing the ensemble of modifications co-occurring with oxidation potentially highlights novel mechanisms for regulation of protein structure and function.

Acknowledgements

Conflict of interest

The authors declare no conflicts of interest.

Appendix A. Supplementary material

Supplementary data associated with this article can be found in the online version at http://dx.doi.org/10.1016/j.redox.2018.04.003.

References

[1] S.C. Huber, S.C. Hardin, Numerous posttranslational modifications provide opportunities for the intricate regulation of metabolic enzymes at multiple levels, Curr. Opin. Plant Biol. 7 (3) (2004) 318–322.

[2] Y.L. Deribe, T. Pawson, I. Dikic, Post-translational modifications in signal integration, Nat. Struct. Mol. Biol. 17 (6) (2010) 666–672.

[3] J.V. Olsen, et al., Global, in vivo, and site-specific phosphorylation dynamics in signaling networks, Cell 127 (3) (2006) 635–648.

[4] C.H. Foyer, G. Noctor, Redox regulation in photosynthetic organisms: signaling, acclimation, and practical implications, Antioxid. Redox Signal. 11 (4) (2009) 861–905.

[5] M. Zaffagnini, et al., Redox regulation in photosynthetic organisms: focus on glutathionylation, Antioxid. Redox Signal. 16 (6) (2012) 567–586.

[6] M. Zaffagnini, et al., Protein S-nitrosylation in photosynthetic organisms: a comprehensive overview with future perspectives, Biochim. Biophys. Acta 1864 (8) (2016) 952–966.

[7] L.B. Poole, K.J. Nelson, Discovering mechanisms of signaling-mediated cysteine oxidation, Curr. Opin. Chem. Biol. 12 (1) (2008) 18–24.

[8] M. Hamann, et al., Quantitation of protein sulfinic and sulfonic acid, irreversibly oxidized protein cysteine sites in cellular proteins, Methods Enzymol. 348 (2002) 146–156.

[9] B.B. Buchanan, Y. Balmer, Redox regulation: a broadening horizon, Annu. Rev. Plant Biol. 56 (2005) 187–220.

[10] T. Hunter, The age of crosstalk: phosphorylation, ubiquitination, and beyond, Mol. Cell 28 (5) (2007) 730–738.

[11] R.S. Rao, et al., Convergent signaling pathways–interaction between methionine oxidation and serine/threonine/tyrosine O-phosphorylation, Cell Stress Chaperones 20 (1) (2015) 15–21.

[12] S.C. Hardin, et al., Coupling oxidative signals to protein phosphorylation via methionine oxidation in Arabidopsis, Biochem. J. 422 (2) (2009) 305–312.

[13] G. Filomeni, G. Rotilio, M.R. Ciriolo, Disulfide relays and phosphorylative cascades: partners in redox-mediated signaling pathways, Cell Death Differ. 12 (12) (2005) 1555–1563.

[14] K.M. Balmant, T. Zhang, S. Chen, Protein phosphorylation and redox modification in stomatal guard cells, Front. Physiol. 7 (26) (2016).

[15] S.Y. Kim, et al., The plastid casein kinase 2 phosphorylates rubisco activase at the Thr-78 site but is not essential for regulation of rubisco activation state, Front. Plant Sci. 7 (2016) 404.

[16] E.E. Burns, et al., Constitutive redox and phosphoproteome changes in multiple herbicide resistant Avena fatua L. are similar to those of systemic acquired resistance and systemic acquired acclimation, J. Plant Physiol. 220 (2018) 105–114.

[17] M. Grabsztunowicz, M.M. Koskela, P. Mulo, Post-translational modifications in regulation of chloroplast function: recent advances, Front. Plant Sci. 8 (240) (2017).

[18] S.S. Merchant, et al., The Chlamydomonas genome reveals the evolution of key animal and plant functions, Science 318 (5848) (2007) 245–250.

[19] M. Zaffagnini, et al., Glutathionylation in the photosynthetic model organism Chlamydomonas reinhardtii: a proteomic survey, Mol. Cell Proteom. 11 (2) (2012) (p. M111.014142).

[20] S. Morisse, et al., Insight into protein S-nitrosylation in Chlamydomonas reinhardtii, Antioxid. Redox Signal. 21 (9) (2014) 1271–1284.

[21] M.E. Perez-Perez, et al., The deep thioredoxome in chlamydomonas reinhardtii: new insights into redox regulation, Mol. Plant 10 (8) (2017) 1107–1125.

[22] W.O. Slade, et al., Quantifying reversible oxidation of protein thiols in photosynthetic organisms, J. Am. Soc. Mass Spectrom. 26 (4) (2015) 631–640.

[23] V. Wagner, et al., Analysis of the phosphoproteome of Chlamydomonas reinhardtii provides new insights into various cellular pathways, Eukaryot. Cell 5 (3) (2006) 457–468.

[24] J. Pan, et al., Protein phosphorylation is a key event of flagellar disassembly revealed by analysis of flagellar phosphoproteins during flagellar shortening in Chlamydomonas, J. Proteome Res. 10 (8) (2011) 3830–3839.

[25] H. Wang, et al., The global phosphoproteome of Chlamydomonas reinhardtii reveals complex organellar phosphorylation in the flagella and thylakoid membrane, Mol. Cell Proteom. 13 (9) (2014) 2337–2353.

[26] E.G. Werth, et al., Probing the global kinome and phosphoproteome in Chlamydomonas reinhardtii via sequential enrichment and quantitative proteomics, Plant J. (2016).

[27] M. Dong, et al., Selective enrichment of cysteine-containing phosphopeptides for subphosphoproteome analysis, J. Proteome Res. 14 (12) (2015) 5341–5347.

[28] U.-B. Kang, W.M. Alexander, J.A. Marto, Interrogating the hidden phosphoproteome, Proteomics 17 (6) (2017) (p. 1600437-n/a).

[29] H. Huang, et al., Simultaneous enrichment of cysteine-containing peptides and phosphopeptides using a cysteine-specific phosphonate adaptable tag (CysPAT) in combination with titanium dioxide (TiO2) chromatography, Mol. Cell Proteom. 15 (10) (2016) 3282–3296.

[30] S.P. Rodrigues, et al., Multiplexing strategy for simultaneous detection of redox-, phospho- and total proteome - understanding TOR regulating pathways in Chlamydomonas reinhardtii, Anal. Methods 7 (17) (2015) 7336–7344.

[31] E.H. Harris, The Chlamydomonas Sourcebook, Academic Press, Inc, San Diego, 1989.

[32] L. Käll, et al., Semi-supervised learning for peptide identification from shotgun proteomics datasets, Nat. Methods 4 (11) (2007) 923–925.

[33] M.M. Savitski, et al., Confident phosphorylation site localization using the Mascot Delta Score, Mol. Cell. Proteom. 10 (2) (2011) (p. M110. 003830).

[34] C. Xie, et al., KOBAS 2.0: a web server for annotation and identification of enriched pathways and diseases, Nucleic Acids Res. 39 (suppl_2) (2011) W316–W322.

[35] F. Supek, et al., REVIGO summarizes and visualizes long lists of gene ontology terms, PLoS One 6 (7) (2011) e21800.

[36] Y. Moriya, et al., KAAS: an automatic genome annotation and pathway reconstruction server, Nucleic Acids Res. 35 (suppl_2) (2007) W182–W185.

[37] M. Kanehisa, et al., KEGG for integration and interpretation of large-scale molecular data sets, Nucleic Acids Res. 40 (D1) (2012) D109–D114.

[38] C. Camacho, et al., BLAST+: architecture and applications, BMC Bioinform. 10 (2009) 421.

[39] J.A. Vizcaino, et al., ProteomeXchange provides globally coordinated proteomics data submission and dissemination, Nat. Biotechnol. 32 (3) (2014) 223–226.

[40] J. Paulech, et al., Large-scale capture of peptides containing reversibly oxidized cysteines by thiol-disulfide exchange applied to the myocardial redox proteome, Anal. Chem. 85 (7) (2013) 3774–3780.

[41] J. Guo, et al., Resin-assisted enrichment of thiols as a general strategy for proteomic profiling of cysteine-based reversible modifications, Nat. Protoc. 9 (1) (2014) 64–75.

[42] M.T. Forrester, et al., Proteomic analysis of S-nitrosylation and denitrosylation by resin-assisted capture, Nat. Biotechnol. 27 (6) (2009) 557–559.

[43] D. Su, et al., Quantitative site-specific reactivity profiling of S-nitrosylation in mouse skeletal muscle using cysteinyl peptide enrichment coupled with mass spectrometry, Free Radic. Biol. Med. 57 (2013) 68–78.

[44] C. Lind, et al., Identification of S-glutathionylated cellular proteins during oxidative stress and constitutive metabolism by affinity purification and proteomic analysis, Arch. Biochem. Biophys. 406 (2) (2002) 229–240.

[45] D. Su, et al., Proteomic identification and quantification of S-glutathionylation in mouse macrophages using resin-assisted enrichment and isobaric labeling, Free Radic. Biol. Med. 67 (2014) 460–470.

[46] M.T. Forrester, et al., Site-specific analysis of protein S-acylation by resin-assisted capture, J. Lipid Res. 52 (2) (2011) 393–398.

[47] R.E. Hansen, J.R. Winther, An introduction to methods for analyzing thiols and disulfides: reactions, reagents, and practical considerations, Anal. Biochem. 394 (2) (2009) 147–158.

[48] A. Rogowska-Wrzesinska, et al., Analysis of protein carbonylation–pitfalls and promise in commonly used methods, Free Radic. Res. 48 (10) (2014) 1145–1162.

[49] H.H. Al-Sa'doni, et al., Neocuproine, a selective Cu(I) chelator, and the relaxation of rat vascular smooth muscle by S-nitrosothiols, Br. J. Pharmacol. 121 (6) (1997) 1047–1050.

[50] Y. Zhang, et al., Protein analysis by shotgun/bottom-up proteomics, Chem. Rev. 113 (4) (2013) 2343–2394.

[51] X. Han, A. Aslanian, J.R. Yates, Mass spectrometry for proteomics, Curr. Opin. Chem. Biol. 12 (5) (2008) 483–490.

[52] R.E. Hansen, D. Roth, J.R. Winther, Quantifying the global cellular thiol-disulfide status, Proc. Natl. Acad. Sci. USA 106 (2) (2009) 422–427.

[53] H. Wang, S. Alvarez, L.M. Hicks, Comprehensive comparison of iTRAQ and label-free LC-based quantitative proteomics approaches using two Chlamydomonas reinhardtii strains of interest for biofuels engineering, J. Proteome Res. 11 (1) (2012) 487–501.

[54] J.R. Wiśniewski, et al., Universal sample preparation method for proteome analysis, Nat. Methods 6 (2009) 359.

[55] B. Domon, R. Aebersold, Options and considerations when selecting a quantitative proteomics strategy, Nat. Biotechnol. 28 (7) (2010) 710–721.

[56] R. Wu, et al., Correct interpretation of comprehensive phosphorylation dynamics requires normalization by protein expression changes, Mol. Cell Proteom. 10 (8) (2011) (p. M111.009654).

[57] X. Yue, A. Schunter, A.B. Hummon, Comparing multistep immobilized metal affinity chromatography and multistep TiO2 methods for phosphopeptide enrichment, Anal. Chem. 87 (17) (2015) 8837–8844.

[58] Y.M. Go, J.D. Chandler, D.P. Jones, The cysteine proteome, Free Radic. Biol. Med. 84 (2015) 227–245.

[59] L. Fu, et al., Systematic and quantitative assessment of hydrogen peroxide reactivity with cysteines across human proteomes, Mol. Cell Proteom. 16 (10) (2017) 1815–1828.

[60] C.C. Winterbourn, Reconciling the chemistry and biology of reactive oxygen species, Nat. Chem. Biol. 4 (5) (2008) 278–286.

[61] J. Peng, et al., A proteomics approach to understanding protein ubiquitination, Nat. Biotechnol. 21 (8) (2003) 921–926.

[62] R.S. Rao, I.M. Moller, Pattern of occurrence and occupancy of carbonylation sites in proteins, Proteomics 11 (21) (2011) 4166–4173.

[63] R.C. Bollineni, R. Hoffmann, M. Fedorova, Proteome-wide profiling of carbonylated proteins and carbonylation sites in HeLa cells under mild oxidative stress conditions, Free Radic. Biol. Med. 68 (Supplement C) (2014) 186–195.

[64] I. Lounifi, et al., Interplay between protein carbonylation and nitrosylation in plants, Proteomics 13 (3–4) (2013) 568–578.

[65] M. Tamaoki, et al., Transcriptome analysis of O3-exposed Arabidopsis reveals that multiple signal pathways act mutually antagonistically to induce gene expression, Plant Mol. Biol. 53 (4) (2003) 443–456.

[66] M. Moore, N. Gossmann, K.-J. Dietz, Redox regulation of cytosolic translation in plants. Trends Plant Sci. 21(5): p. 388–397.

[67] J. Minagawa, State transitions—The molecular remodeling of photosynthetic supercomplexes that controls energy flow in the chloroplast, Biochim. Biophys. Acta - Bioenerg. 1807 (8) (2011) 897–905.

[68] P. Pesaresi, et al., Dynamics of reversible protein phosphorylation in thylakoids of flowering plants: the roles of STN7, STN8 and TAP38, Biochim. Biophys. Acta 1807 (8) (2011) 887–896.

[69] M. Pribil, et al., Role of plastid protein phosphatase TAP38 in LHCII dephosphorylation and thylakoid electron flow, PLoS Biol. 8 (1) (2010) e1000288.

[70] S. Morisse, et al., Thioredoxin-dependent redox regulation of chloroplastic phosphoglycerate kinase from Chlamydomonas reinhardtii, J. Biol. Chem. 289 (43) (2014) 30012–30024.

[71] S.D. Lemaire, et al., Thioredoxins in chloroplasts, Curr. Genet. 51 (6) (2007) 343–365.

[72] R.P. Dunford, et al., Purification of active chloroplast sedoheptulose-1,7-bisphosphatase expressed in Escherichia coli, Protein Expr. Purif. 14 (1) (1998) 139–145.

[73] F. Sparla, P. Pupillo, P. Trost, The C-terminal extension of glyceraldehyde-3-phosphate dehydrogenase subunit B acts as an autoinhibitory domain regulated by thioredoxins and nicotinamide adenine dinucleotide, J. Biol. Chem. 277 (47) (2002) 44946–44952.

[74] S. Baginsky, Protein phosphorylation in chloroplasts - a survey of phosphorylation targets, J. Exp. Bot. 67 (13) (2016) 3873–3882.

[75] A.R. Portis Jr., Rubisco activase - Rubisco's catalytic chaperone, Photosynth. Res. 75 (1) (2003) 11–27.

[76] M.E. Salvucci, J.C. Anderson, Factors affecting the activation state and the level of total activity of ribulose bisphosphate carboxylase in tobacco protoplasts, Plant Physiol. 85 (1) (1987) 66–71.

[77] B. Gontero, M.E. Salvucci, Regulation of photosynthetic carbon metabolism in aquatic and terrestrial organisms by Rubisco activase, redox-modulation and CP12, Aquat. Bot. 118 (2014) 14–23.

[78] S. Lemeille, et al., Stt7-dependent phosphorylation during state transitions in the green alga Chlamydomonas reinhardtii, Mol. Cell Proteom. 9 (6) (2010) 1281–1295.

[79] L. Marri, et al., In vitro characterization of Arabidopsis CP12 isoforms reveals common biochemical and molecular properties, J. Plant Physiol. 167 (12) (2010) 939–950.

[80] N. Wedel, J. Soll, B.K. Paap, CP12 provides a new mode of light regulation of Calvin cycle activity in higher plants, Proc. Natl. Acad. Sci. USA 94 (19) (1997)

10479–10484.

[81] R. Groben, et al., Comparative sequence analysis of CP12, a small protein involved in the formation of a Calvin cycle complex in photosynthetic organisms, Photosynth. Res. 103 (3) (2010) 183–194.

[82] I. Couso, et al., Synergism between inositol polyphosphates and TOR kinase signaling in nutrient sensing, growth control, and lipid metabolism in Chlamydomonas, Plant Cell 28 (9) (2016) 2026–2042.

[83] S. Mulugu, et al., A conserved family of enzymes that phosphorylate inositol hexakisphosphate, Science 316 (5821) (2007) 106–109.

[84] M.E. Pérez-Pérez, et al., Monitoring autophagy in the model green microalga Chlamydomonas reinhardtii, Cells 6 (4) (2017) 36.

[85] A.V. Budanov, Stress-responsive sestrins link p53 with redox regulation and mammalian target of rapamycin signaling, Antioxid. Redox Signal. 15 (6) (2011) 1679–1690.

[86] S. Yoshida, et al., Redox regulates mammalian target of rapamycin complex 1 (mTORC1) activity by modulating the TSC1/TSC2-Rheb GTPase pathway, J. Biol. Chem. 286 (37) (2011) 32651–32660.

[87] T.J. van Dam, et al., Evolution of the TOR pathway, J. Mol. Evol. 73 (3–4) (2011) 209–220.

[88] J.L. Crespo, BiP links TOR signaling to ER stress in Chlamydomonas, Plant Signal.

Behav. 7 (2) (2012) 273–275.

[89] J. Kim, et al., AMPK and mTOR regulate autophagy through direct phosphorylation of Ulk1, Nat. Cell Biol. 13 (2) (2011) 132–141.

[90] M.E. Pérez-Pérez, S.D. Lemaire, J.L. Crespo, Reactive oxygen species and autophagy in plants and algae, Plant Physiol. 160 (1) (2012) 156–164.

[91] A. Shemi, S. Ben-Dor, A. Vardi, Elucidating the composition and conservation of the autophagy pathway in photosynthetic eukaryotes, Autophagy 11 (4) (2015) 701–715.

[92] A. Schweighofer, H. Hirt, I. Meskiene, Plant PP2C phosphatases: emerging functions in stress signaling, Trends Plant Sci. 9 (5) (2004) 236–243.

[93] V. Wagner, et al., The phosphoproteome of a Chlamydomonas reinhardtii eyespot fraction includes key proteins of the light signaling pathway, Plant Physiol. 146 (2) (2008) 772–788.

[94] I. Meskiene, et al., Stress-induced protein phosphatase 2C is a negative regulator of a mitogen-activated protein kinase, J. Biol. Chem. 278 (21) (2003) 18945–18952.

[95] A. Kulik, et al., SnRK2 protein kinases—key regulators of plant response to abiotic stresses, Omics: J. Integr. Biol. 15 (12) (2011) 859–872.

[96] D. Gonzalez-Ballester, et al., The central role of a SNRK2 kinase in sulfur deprivation responses, Plant Physiol. 147 (1) (2008) 216–227.